

## LINEAR POLARIZATION OBSERVATIONS OF WATER MASERS IN W3 IRS 5

HIROSHI IMAI,<sup>1,2,3,4</sup> SHINJI HORIUCHI,<sup>5,6</sup> SHUJI DEGUCHI,<sup>7</sup> AND OSAMU KAMEYA<sup>1,2</sup>

Received 2003 April 13; accepted 2003 May 28

### ABSTRACT

We present a magnetic field mapping of water maser clouds in the star-forming region W3 IRS 5, which has been made on the basis of the linear polarization VLBI observation. Using the Very Long Baseline Array at 22.2 GHz, 16 of 61 detected water masers were found to be linearly polarized with polarization degrees up to 13%. Although 10 polarized features were widely distributed in the whole W3 IRS 5 water maser region, they had position angles similar to the magnetic field vectors ( $\sim 75^\circ$  east from the north). The magnetic field vectors are roughly perpendicular to the spatial alignments of the maser features. They are consistent with the hourglass model of the magnetic field, which was previously proposed to explain the magnetic field in the whole W3 Main region ( $r \sim 0.1$  pc). They are, on the other hand, not aligned to the directions of maser feature proper motions observed previously. This implies that the W3 IRS 5 magnetic field was controlled by a collapse of the W3 Main molecular cloud rather than by the outflow originated from W3 IRS 5.

*Subject headings:* ISM: individual (W3 IRS 5) — ISM: jets and outflows — masers — stars: formation

### 1. INTRODUCTION

The birth of massive stars is characterized by a collapse of the molecular cloud core when self-gravity overwhelms the magnetic pressure in the core as a result of magnetic field dilution. In this situation, the core is no longer supported by magnetic field pressure in the cloud and is called “magnetically supercritical” (e.g., Shu, Adams, & Lizano 1987; Feigelson & Montmerle 1999, and references therein). Measurements of the magnetic field strengths and directions in star-forming regions have been made in a variety of spatial scales, from whole star-forming regions (1–10 pc) down to individual molecular cloud cores (e.g., Heiles et al. 1993; McKee et al. 1993; Evans 1999, and references therein). On a smaller scale, the measurements were made mainly with radio interferometers with higher angular resolution. However, because of the complicated structures of the magnetic fields expected from the presence of the dense clumps and outflows, and because of the uncertainty in calibration in the polarimetric interferometry, it is more difficult to map the magnetic field accurately on this scale.

Water maser emission is often associated with star-forming regions (SFRs) with energetic outflows from young stellar objects (YSOs) (e.g., Elitzur 1992a, 1992b and references therein). VLBI observations have revealed that water maser emission consists of clusters of compact maser features with a typical size of 1 AU and a velocity width of 1 km s<sup>-1</sup> (e.g., Reid & Moran 1981). Measurements of Doppler velocities and proper motions of maser features have led to the conclusion that the spatial motions of maser

features really reflect the true three-dimensional gas kinematics (e.g., Gwinn, Moran, & Reid 1992; Torrelles et al. 2001a, 2001b). Previous observations have found expansion motions produced by outflows from YSOs or expanding H II regions (e.g., Imai et al. 2000, hereafter Paper I, and references therein). Shocks, which have velocities exceeding about 20 km s<sup>-1</sup> and are running into high-density ( $n_{\text{H}_2} \geq 3 \times 10^6$  cm<sup>-3</sup>) magnetized material, successfully explain the water maser emission associated with energetic YSO outflows (e.g., Hollenbach & McKee 1989; Elitzur, Hollenbach, & McKee 1989, 1992; Hollenbach, Elitzur, & McKee 1993).

Polarimetric mapping of individual water maser features was made for the first time using VLBI data in W51 M by Leppänen, Liljeström, & Diamond (1998, hereafter LLD; see also in Orion KL, Matveyenko, Diamond, & Graham 2003). They found that the observed directions of linear polarization were well aligned along a stream of water maser features found in W51 M. It should be noted that the observed direction of the linear polarization does not directly indicate the magnetic field direction of the cloud because it depends on the angle between the magnetic field and the photon propagation direction (toward an observer) (e.g., Goldreich, Keeley, & Kwan 1973; Deguchi & Watson 1986b, 1990). In the case of W51 M, the observed directions of linear polarization were interpreted to be parallel to the magnetic field vector projected on the sky plane because the field vector is expected to be roughly tangential to the line of sight due to coupling with the Sagittarius spiral arm. LLD concluded that the alignment of the water maser linear polarization was created by shocks caused by the nearby expanding H II region. The linear polarization of water masers as a tracer of the interstellar magnetic fields is indirectly supported by the fact that the linear polarization directions in a maser region are stable on a timescale of several years despite the much shorter lifetimes and timescale of flux variability of maser features (Abraham & Vilas Boas 1994; LLD; Horiuchi, Miggenes, & Deguchi 2000; Horiuchi & Kameya 2000; Horiuchi & Kemaya 2003).

This paper discusses the results of the magnetic field mapping of water maser clouds in the massive star-forming region W3 IRS 5 revealed by a VLBI observation. W3 IRS 5

<sup>1</sup> Mizusawa Astrogeodynamics Observatory, National Astronomical Observatory, Mizusawa, Iwate 023-0861, Japan.

<sup>2</sup> VLBI Exploration of Radio Astrometry Project Office, National Astronomical Observatory, Mitaka, Tokyo 181-8588, Japan.

<sup>3</sup> Joint Institute for VLBI in Europe, Postbus 2, 7990 AA Dwingeloo, Netherlands.

<sup>4</sup> Current address: Department of Physics, Faculty of Science, Kagoshima University, 1-21-35 Korimoto, Kagoshima 890-0065, Japan.

<sup>5</sup> VLBI Space Observatory Programme Project Office, National Astronomical Observatory, Mitaka, Tokyo 181-8588, Japan.

<sup>6</sup> Jet Propulsion Laboratory, 4800 Oak Grove Drive, Pasadena, CA 91109.

<sup>7</sup> Nobeyama Radio Observatory, National Astronomical Observatory, Minamimaki, Minamisaku, Nagano 384-1305, Japan.

is considered to be at the very early phase of star formation because of the lack of high-velocity components in the water masers, as suggested by Genzel & Downes (1977). Previous observations also supported this interpretation of W3 IRS 5 (e.g., Claussen et al. 1994; Tieftrunk et al. 1997; Roberts, Crutcher, & Troland 1997). In a  $2'' \times 3''$  field of W3 IRS 5, Claussen et al. (1994) and Tieftrunk et al. (1997) found the distribution of a cluster of centimeter-continuum emission sources. Imai et al. (2000) investigated the three-dimensional kinematics of the water masers in W3 IRS 5 and estimated a distance to this region to be  $1.83 \pm 0.14$  kpc. In the present paper, the value of 1.8 kpc is adopted as the distance to W3 IRS 5. Imai, Deguchi, & Sasao (2002, hereafter Paper II) investigated the physical condition of the region where the water masers are excited. They found that turbulent motions dominate the morphology and kinematics on a microscopic scale (down to 0.01 AU). Figure 1 shows the distribution and proper motions of the water maser features found in Paper I.

Troland et al. (1989) and Roberts et al. (1993, hereafter RCTG) measured the Zeeman effect of the  $H_1$  line in W3 IRS 5. They revealed the magnetic field projected along the line of sight on a scale of  $\sim 0.6$  pc and demonstrated an “hourglass” model of the magnetic field. The above scale is roughly equivalent to the core size found in this cloud discovered in the  $^{13}\text{CO}$  line by Hayashi, Kobayashi, & Hasegawa (1989). A pinch of the hourglass was found to be located very close to W3 IRS 5 region and to have a magnetic field strength higher than 1 mG. Greaves, Murray, & Holland (1994) also made a polarimetric observation at sub-millimeter wavelengths and estimated the magnetic field in W3 IRS 5 on a scale of 0.1 pc; the result supports the hourglass model. Barvainis & Deguchi (1989) found that the W3 IRS 5 water masers were highly linearly polarized. Sarma, Troland, & Romney (2001, hereafter STR) and Sarma et al. (2002, hereafter STCR) measured the Zeeman effect of the bright components of the water masers and estimated the magnetic field strength along the line of sight to be  $\sim 30$  mG.

In the present paper, we focus on whether the magnetic field measured in water masers traces that found on the larger scale. The cause that determines the shape of the large-scale magnetic field is also speculated on: either the collapse of the parent molecular cloud or the formation of a magnetohydrodynamical jet. Section 2 describes the polarimetric observations using the Very Long Baseline Array (VLBA) and the Very Large Array (VLA) of the National Radio Astronomy Observatory (NRAO)<sup>8</sup> and data reduction. The results are presented in § 3. Section 4 mainly discusses the relation between the measured directions of maser linear polarization and possible directions and strength of the magnetic field in the observed scale ( $<5''$ ) of W3 IRS 5.

## 2. OBSERVATIONS AND DATA REDUCTION

The polarimetric observation of water masers in W3 IRS 5 was made on 1998 November 21 using 10 telescopes of the VLBA. The water masers and calibrators (NRAO 150, JVAS 0212+735, and 0423-014) were observed for 10 hr total. The observed signals were recorded in a 4 MHz base band channel with both right- and left-circular polarization

<sup>8</sup> The NRAO is a facility of the US National Science Foundation, operated under a cooperative agreement by Associated Universities, Inc.

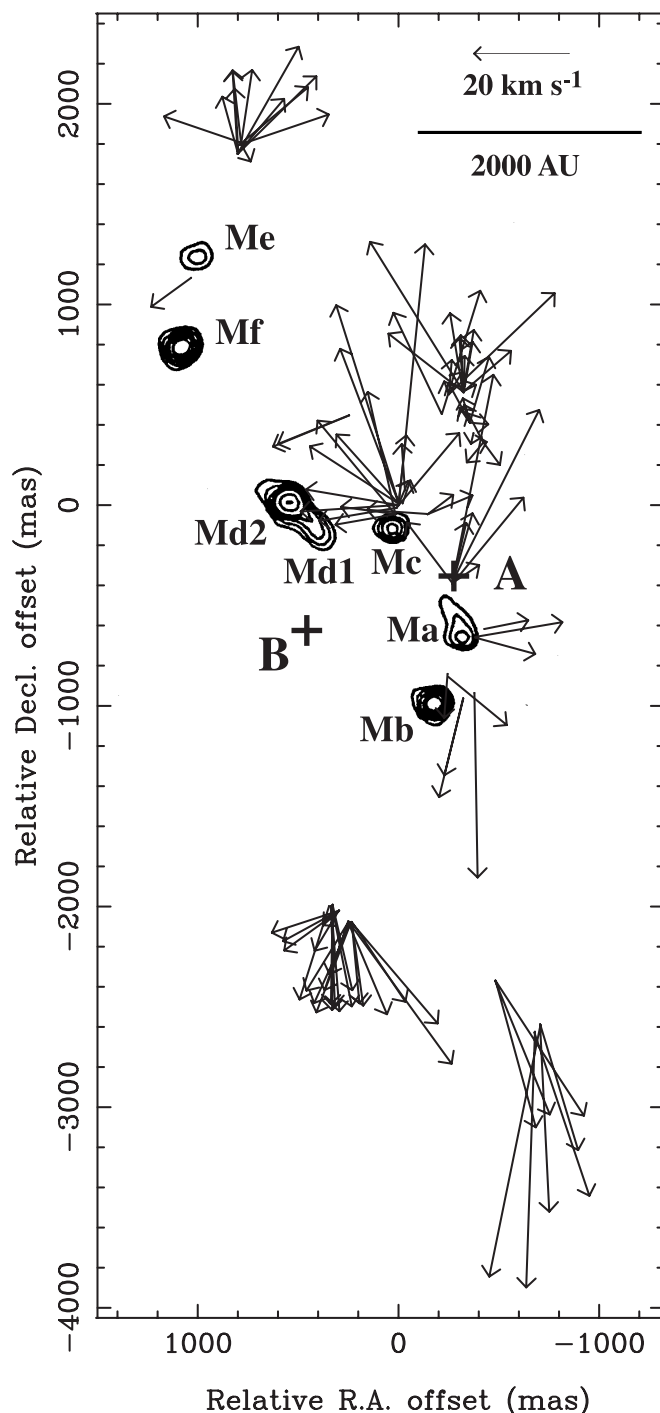


FIG. 1.—Water maser features observed in Paper I and compact radio continuum sources observed by Claussen et al. (1994) in W3 IRS 5. Arrows indicate locations and proper motions of water maser features. The arrow length indicates the magnitude of the proper motion per year ( $\times 325$ ), respectively. The radio continuum sources, presented in Fig. 1 of Claussen et al. (1994), are shown as contours. The designations of the continuum sources are the same as those in Tieftrunk et al. (1997). The two plus marks A and B indicate the locations of the driving sources of the outflows in W3 IRS 5, which were estimated in Paper I.

(RCP, LCP) in 2 bit sampling. The recorded data were correlated with the VLBA correlator in Socorro, New Mexico, which yielded parallel and cross-hand visibilities with 128 spectral channels. The correlated data covered a velocity range of  $-58 \text{ km s}^{-1} \leq V_{\text{LSR}} \leq -5 \text{ km s}^{-1}$  and a velocity spacing of  $0.42 \text{ km s}^{-1}$  per spectral channel.

Data calibration and imaging were mostly made using the procedures in AIPS.<sup>9</sup> First, the data of the parallel-hand-polarization visibilities were reduced in the usual procedures (e.g., Reid 1995; Diamond 1995) and fringe fitting, self-calibration, and complex bandpass solutions were obtained independently in RCP and LCP. Although the water maser emission was strong enough to apply the “template method” to calibrate the visibility amplitudes (Diamond 1995), the bandwidth of 4 MHz was too narrow to obtain a sufficient number of emission-free velocity channels in the template total-power spectrum of the maser emission. Instead, we applied tables of the measured system noise temperatures and antenna gains. In the self-calibration, we obtained a Stokes  $I$  maser map of the velocity component (maser spot) at  $-40.2 \text{ km s}^{-1}$  and complex gain solutions every 6 s.

Second, the instrumental polarization parameters ( $D$ -terms) of the telescopes were obtained using the AIPS RUN script CROSSPOL and the task LPCAL with scans of 0420–014, which is well linearly polarized. The  $D$ -term solutions were applied to the maser data. After the  $D$ -term calibration, the Stokes  $I$ ,  $Q$ ,  $U$  maps of maser spots were obtained independently. The naturally weighted synthesized beam was  $0.68 \times 0.49 \text{ mas}$ , with the major axis at a position angle P.A. =  $3^\circ.3$ . No smoothing in velocity channel was applied. The detection limit of about  $30 \text{ mJy beam}^{-1}$  at a  $5 \sigma$  noise was obtained in velocity channels without bright maser emission. Before making the final image cubes, we looked for the masers by making wider maps covering a  $2'' \times 5''$  field with a larger synthesized beam.

Third, each velocity component (maser spot; see e.g., Gwinn 1994a, 1994b; Paper II) in the image cube was fitted by a two-dimensional Gaussian brightness distribution using the AIPS task JMFIT. The uncertainty of the estimated position due to thermal noise was 3 microarcseconds ( $\mu\text{as}$ ) for a 1 Jy spot. On the other hand, positional accuracy of the brightness peak of a maser feature (a cluster of maser spots) depends on the distribution of maser spots in the feature and the brightness distributions of the maser spots and limited to be typically  $10 \mu\text{as}$ . The electric vector position angle (EVPA; see LLD)  $\text{EVPA} = \arctan(Q/U)/2$  of each maser spot was calculated from the Stokes  $Q$  and  $U$  parameters. For each maser feature (a cluster of maser spots existing together within 1 mas and  $1 \text{ km s}^{-1}$  in position and velocity; Papers I and II), the degree of linear polarization and the EVPA were obtained from the Stokes parameters ( $I$ ,  $Q$ ,  $U$ ) of the intensity peak in the maser feature.

The water masers were also observed with the VLA (26 antennas) in the C configuration on 1998 November 28, 1 week later than the VLBA observation. The water masers and calibrators (3C 48, 0420–014, and 3C 138) were scanned for 2 hr total. The observed signals were recorded in a 3 MHz base band with both right- and left-circular polarization. The correlated data had 64 spectral channels with a velocity spacing of  $0.63 \text{ km s}^{-1}$  per spectral channel. The  $D$ -terms of the antennas were obtained from the scans of 3C 48, which covered a variation of parallactic angle over  $180^\circ$ , assuming the intrinsic EVPA of  $-72^\circ.5$ . Then we confirmed that the obtained EVPAs of 3C 138 and 0420–024 were consistent with those previously obtained by Akujor et al. (1993) and Marscher et al. (2002), respectively.

The EVPA at  $V_{\text{LSR}} = -42.2 \text{ km s}^{-1}$  in the maser feature W3 IRS 5:12003 5 (see Table 1) was compared for the VLA and VLBA data. At this velocity, the maser spot was most prominent and its polarimetric parameters were well determined. A correction ( $\Delta\text{EVPA} = 39^\circ.3$ ) was applied to the EVPAs obtained with the VLBA. Taking into account the variation of EVPA in the maser feature ( $\leq 3^\circ$ ), the ambiguity of the assumed EVPA of 3C 48 ( $\sim 5^\circ$ ), and the accuracy of the calibration of the VLA data (uncertainty in R–L phase determination,  $\leq 0^\circ.3$ ), the accuracy of EVPA was expected to be  $\sim 6^\circ$ . Because the VLA observation was made 7 days after the VLBA observation, the estimated EVPAs might suffer from the EVPA time variation of the feature W3 IRS 5:12003 5.

### 3. RESULTS

We detected 61 maser features consisting of 290 maser spots. These numbers are smaller by factors of 2–3 and 4–7, respectively, than those in the previous VLBA observations (Paper I; see also Paper II) while the sensitivity of the present observation was better than that of the previous ones. The decrease of features was likely due to less activity in maser excitation, while the decrease of spots was due to lower velocity resolution by a factor of 4 in the present observation.

Table 1 summarizes the parameters of water maser features in W3 IRS 5. Only 15 of 61 features had proper motions that were measured previously in Paper I. It was difficult to identify the same features between the observations of Paper I and the present work because many features were likely to appear and disappear in the crowded regions during the epoch separation of 11 months. The highest degrees of polarization was 13% in the present observation, which was smaller than those (up to 30%) found in a previous single-dish observation (Barvainis & Deguchi 1989) and our unpublished VLBI observation with a 400 km baseline. As shown in Figure 2, no correlation was found

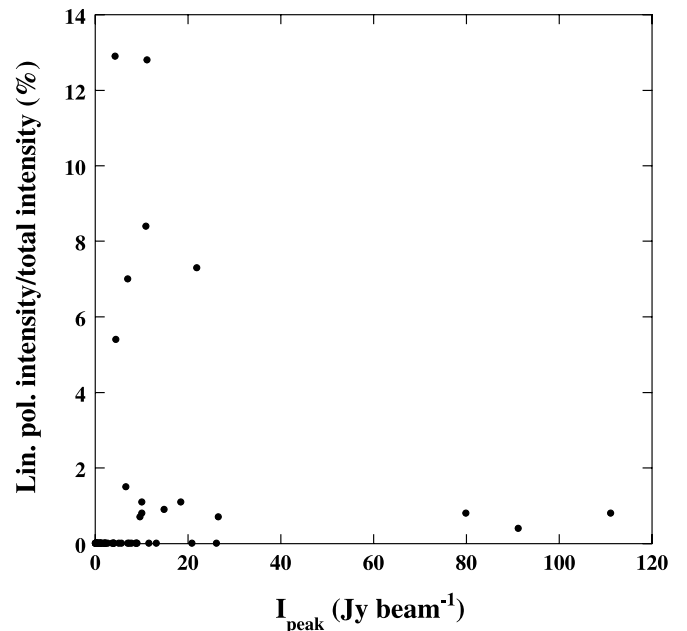


Fig. 2.—Distribution of polarization degrees of maser features against their peak intensities.

<sup>9</sup> The NRAO Astronomical Imaging Processing System.

TABLE 1  
PARAMETERS OF THE WATER MASER FEATURES TOWARD W3 IRS 5

MASER FEATURE <sup>a</sup> (W3 IRS 5: I2003)	OFFSET <sup>b</sup>		LSR VELOCITY (km s <sup>-1</sup> )		PEAK INTENSITY (Jy beam <sup>-1</sup> )	$\mathcal{P}^d$ (%)	EVPA (deg)	MASER FEATURE <sup>e</sup> (W3 IRS 5: I2000)
	R.A. (mas)	Decl. (mas)	Peak	Width <sup>c</sup>				
1.....	-1.50	3.33	-56.0	1.7	0.04	...	...	...
2.....	1075.72	1016.29	-43.1	3.8	18.41	11.0	-12.1	...
3.....	-389.93	-661.34	-42.9	1.7	7.78	...	...	...
4.....	0.08	-0.99	-42.6	1.3	6.95	...	...	...
5.....	-1.49	3.36	-42.1	3.8	111.05	0.8	-15.1	...
6.....	-388.32	-665.56	-42.0	2.1	9.60	0.7	19.8	...
7.....	-388.08	-671.67	-41.7	0.8	3.63	...	...	...
8.....	-431.85	-620.46	-41.7	0.8	1.48	...	...	29
9.....	-387.87	-667.89	-41.3	0.4	0.50	...	...	...
10.....	-0.01	-0.09	-41.3	1.3	26.10	...	...	...
11.....	-18.42	0.16	-40.7	1.7	8.95	...	...	...
12.....	-17.26	-1.79	-40.5	1.3	2.63	...	...	...
13.....	-1.37	4.38	-40.5	1.7	8.69	...	...	...
14.....	0.00	0.00	-40.5	5.1	79.89	0.8	-14.9	...
15.....	-1.66	5.47	-40.3	1.3	8.91	...	...	...
16.....	-0.37	-11.64	-40.0	2.5	20.81	...	...	...
17.....	-3.92	5.23	-39.6	0.4	5.05	...	...	...
18.....	-387.50	-670.38	-39.3	4.2	9.99	0.8	-17.8	...
19.....	-386.67	-677.37	-38.9	3.0	7.25	...	...	...
20.....	-4.28	8.23	-38.8	1.3	5.63	...	...	...
21.....	-3.78	7.50	-38.8	0.8	3.91	...	...	...
22.....	-6.27	8.67	-38.2	3.8	26.49	0.7	-11.8	...
23.....	9.72	-16.39	-37.8	2.1	11.11	12.8	-11.4	...
24.....	-386.73	-676.74	-37.7	1.3	0.29	...	...	...
25.....	-7.97	13.24	-37.5	1.7	1.88	...	...	...
26.....	-9.20	14.11	-36.9	1.7	2.14	...	...	...
27.....	786.55	1792.69	-36.7	2.1	10.01	1.1	-15.5	64
28.....	797.51	1750.03	-36.2	0.8	0.56	...	...	65
29.....	783.13	1802.02	-35.8	3.8	14.81	0.9	-18.0	66
30.....	787.03	1794.17	-35.5	5.1	91.10	0.4	-12.5	63
31.....	328.54	-2001.74	-35.0	1.7	2.24	...	...	71
32.....	796.47	1750.38	-35.0	3.0	0.53	...	...	...
33.....	-416.12	-600.11	-34.6	4.2	11.55	...	...	...
34.....	-1.46	3.30	-34.6	0.4	0.11	...	...	...
35.....	-0.02	-0.02	-34.6	0.4	0.06	...	...	...
36.....	-6.21	8.51	-34.6	0.4	0.08	...	...	...
37.....	794.01	1751.23	-34.5	0.4	2.10	...	...	...
38.....	794.65	1750.92	-34.1	0.4	0.23	...	...	79
39.....	295.92	-2025.00	-33.9	1.7	0.94	...	...	73
40.....	294.72	-2025.82	-33.8	2.5	4.43	5.4	-5.0	76
41.....	293.69	-2027.11	-33.7	0.8	1.06	...	...	...
42.....	331.95	-2004.59	-33.7	1.3	6.95	7.0	89.6	...
43.....	325.76	-1999.60	-33.6	4.6	21.89	7.3	30.4	82
44.....	332.52	-2004.95	-33.3	0.8	4.25	12.9	-79.2	...
45.....	-415.21	-602.42	-33.2	3.0	1.00	...	...	...
46.....	334.25	-2006.04	-33.1	3.0	10.90	8.4	-59.1	83
47.....	-415.45	-604.25	-33.0	3.4	3.84	...	...	...
48.....	324.56	-1998.90	-32.9	5.9	13.12	...	...	...
49.....	324.99	-1998.91	-32.4	2.1	6.56	1.5	-62.5	...
50.....	795.87	1750.48	-32.3	2.1	1.93	...	...	...
51.....	326.65	-1999.60	-32.0	1.3	0.19	...	...	77
52.....	331.83	-2004.52	-31.2	0.4	0.05	...	...	...
53.....	249.87	-2079.93	-30.4	4.6	4.02	...	...	91
54.....	228.02	-2083.62	-29.9	1.7	1.05	...	...	94
55.....	230.35	-2083.38	-29.9	0.8	0.44	...	...	98
56.....	229.26	-2083.48	-29.9	0.4	0.01	...	...	...
57.....	227.05	-2083.52	-29.9	1.7	1.09	...	...	...
58.....	325.72	-1999.57	-29.6	2.1	0.06	...	...	...
59.....	795.39	1750.80	-29.5	1.3	0.13	...	...	...
60.....	-503.83	-2377.04	-23.8	3.0	0.58	...	...	...
61.....	-205.57	-1830.29	-6.8	2.1	1.32	...	...	...

<sup>a</sup> Water maser features detected toward W3 IRS 5. The feature is designated as W3 IRS 5:I2003  $N$ , where  $N$  is the ordinal source number given in this column (I2003 stands for sources found by Imai et al. and listed in 2003).

<sup>b</sup> Relative value with respect to the location of the position-reference maser feature: W3 IRS 5:I2003 14.

<sup>c</sup> Channel velocity spacing multiplied by the number of detected maser spots in the feature.

<sup>d</sup> Fraction of linear polarization intensity to total intensity.

<sup>e</sup> The feature identical to that found in Paper I, W3 IRS 5:I2000  $M$ , where  $M$  is the ordinal source number given in this column.

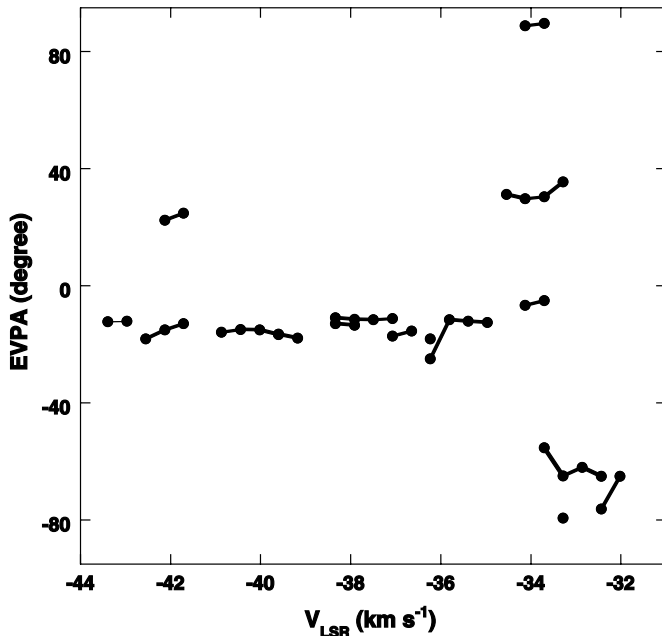


FIG. 3.—Distribution of EVPAs of maser spots against their Doppler velocities. A filled circle shows the maser spot detected its linear polarization. Maser spots in the same maser feature are connected to each other by a thick line.

between a feature intensity and a degree of linear polarization. LLD found a systematic change of EVPAs in a single maser feature at the full velocity width  $\Delta V = 1.3 \text{ km s}^{-1}$ . On the other hand, as shown in Figure 3, EVPAs were almost the same (within  $15^\circ$ ) in all of the features with measured linear polarization in W3 IRS 5.

Figure 4 presents the spatial distribution and the linear polarization directions of the maser features. The present maser map was easily overlaid on the previous ones in Paper I. We found that a cluster of maser features is elongated in the northwest and southeast directions and that the radial velocities have been almost the same among previous maser maps of Papers I and II and the present one (Fig. 4c). Very likely this cluster corresponds to the cluster of maser features with the measured Zeeman effect (the features in Fig. 1 of STR; see also STCR). As STR mentioned, the cluster was located very close to the radio continuum source “c” (Claussen et al. 1994, see Fig. 1). It was quite difficult, however, to exactly identify the same features from one observing epoch to another because the time spans between the two observations were too large ( $\geq 14$  months).

The observed EVPAs were roughly the same among distant maser features (see the features in Figs. 4b and 4c) within a separation of 3800 AU, as well as adjacent maser features within 100 AU. Figure 3 shows that 10 of 16 polarized features exhibited this tendency. The EVPAs were also constant at  $-13^\circ \pm 5^\circ$  in the individual features. The exception was found in the cluster of features seen in Figure 4e, in which EVPAs changed by  $90^\circ$ . Only one feature at the southwest corner of the cluster, W3 IRS 5:I2003 40, had an EVPA roughly equal to those in other clusters.

In W51 M (LLD) and in Orion KL (Matreyenko et al. 2003), EVPAs of masers are well aligned along the direction of a highly collimated flow. In W3 IRS 5, on the other hand, EVPAs are not parallel to the direction of the whole out-

flows, which is oriented at P.A.  $\sim 10^\circ$  (see Figs. 1 and 6 of Paper I). In addition, they are not aligned in the direction of the large-scale CO outflow (P.A.  $\sim 50^\circ$ ; Mitchell, Maillard, & Hasegawa 1991; Hasegawa et al. 1994). Note that the alignment of EVPAs observed in the present paper appears more evident than the alignment of proper motions observed in Paper I. This is probably because the random motions are dominant in the proper motions.

## 4. DISCUSSION

### 4.1. Relation between the EVPA and the Magnetic Field

The present work investigates for the first time the magnetic field of the whole water maser regions covering a large mapping area ( $2'' \times 5''$ ) and the wide maser velocity range ( $\Delta V = 53 \text{ km s}^{-1}$ ). Despite proper motions that have quite different PAs among the maser features, we found the similar EVPA values ( $-13.7^\circ [\pm 3.7^\circ]$  in median) among 10 maser features widely distributed in the whole maser region. This position angle should be perpendicular or parallel to the magnetic field in the water maser region of W3 IRS 5.

A maser theory suggests that the directions of the linear polarization of saturated masers should be perpendicular (or parallel) to the magnetic field projection on the sky if the inclination angle of the magnetic field with respect to the line of sight is  $|\theta_M| \geq 55^\circ$  (or  $|\theta_M| \lesssim 55^\circ$ ) (Goldreich et al. 1973; Deguchi & Watson 1986b). This inclination angle was roughly estimated from the observable parameter  $Q/I$  (see Fig. 2 of Deguchi & Watson 1986a). We estimated the inclination angle to be  $45^\circ \leq \theta_M \leq 60^\circ$  for the observed value  $|Q/I| \lesssim 0.15$ , which is close to the critical inclination angle mentioned above ( $\sim 55^\circ$ ). We expect that the feature at the southwest corner of the cluster, W3 IRS 5:I2003 40, exhibits a “flip” of the linear polarization direction by  $\sim 90^\circ$  because the magnetic field has an inclination angle close to the critical value. However, in other features, we favor  $|\theta_M| \geq 55^\circ$  because the magnetic field on the larger scale is almost tangential to the sky plane, as mentioned above. Thus, the magnetic field projection was estimated to have P.A.  $\sim 76^\circ$ . In contrast, the directions of linear polarization in the W51 M water maser are considered to be parallel to the magnetic field (LLD).

Note that the linear polarization is affected more or less by Faraday rotation due to free electrons in the interstellar medium along the line of sight. We evaluated Faraday rotation for the maser linear polarization at 1.35 cm wavelength,  $\Phi$ , using the following equation,

$$\Phi \simeq 1.48 \times 10^2 D n_e H_{\parallel} , \quad (1)$$

where  $D$  (pc) is the size of an interstellar cloud,  $n_e$  ( $\text{cm}^{-3}$ ) is the number density of free electrons, and  $H_{\parallel}$  (G) is the magnetic field strength along the line of sight. For the cases of a maser cloud ( $D \sim 10^{-4}$  pc,  $n_e \sim 1 \text{ cm}^{-3}$ ,  $H_{\parallel} \sim 30$  mG), a molecular cloud ( $D \sim 0.1$  pc,  $n_e \sim 1 \text{ cm}^{-3}$ ,  $H_{\parallel} \sim 100 \mu\text{G}$ ), and the interstellar space between the W3 region and the Sun ( $D \sim 1.8$  kpc,  $n_e \sim 10^{-2} \text{ cm}^{-3}$ ,  $H_{\parallel} \sim 10 \mu\text{G}$ ), we obtain  $\Phi \sim 4.4 \times 10^{-4}$ ,  $1.5 \times 10^{-3}$ , and  $2.7 \times 10^{-2}$  rad, respectively, which are negligible effects. Although the hypercompact H II regions found in the W3 IRS 5 region ( $D \sim 2 \times 10^{-3}$  pc,  $n_e \sim 1.3 \times 10^5 \text{ cm}^{-3}$ ,  $H_{\parallel} \sim 30$  mG; Claussen et al. 1994) might introduce the strongest Faraday rotation ( $\Phi \sim 120$  rad), they are not located in front of or behind the water maser features with linear polarization.

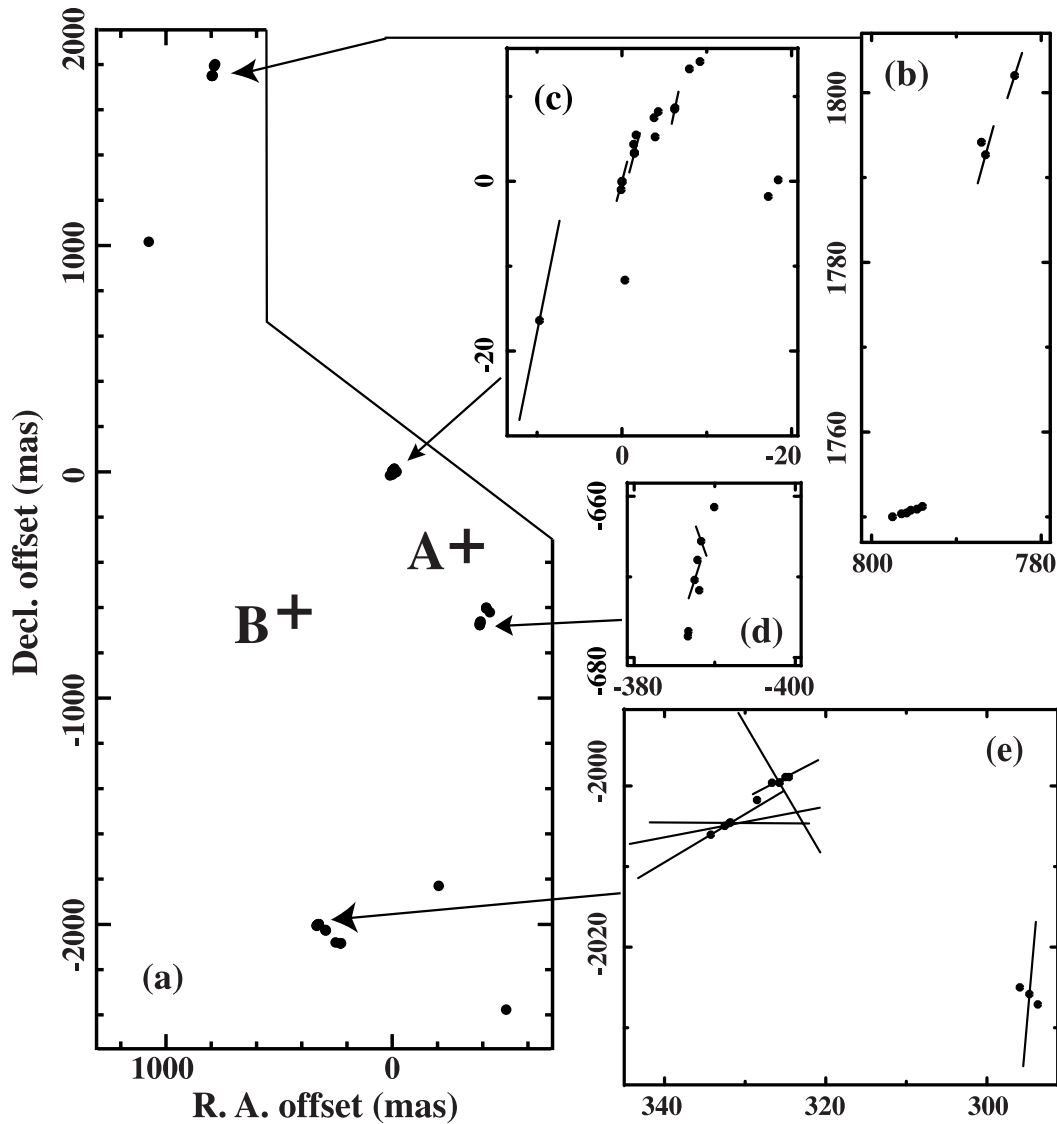


FIG. 4.—Map of linearly polarized maser features in W3 IRS 5. (a) Locations of the maser features (filled circle) detected on 1998 November 21. The two plus marks are the same as those in Fig. 1. The locations of the maser features were estimated with respect to the driving sources of the outflows by assuming a stable distribution of clusters of maser features among observations made in the previous (Paper I) and present works. The location uncertainty of the A outflow is within 100 mas. (b–e) Details of the feature distribution and the directions of the linear polarization of the features. The length and the position angle of a bar indicate a logarithmic scale of the degree of the linear polarization and the EVPA, respectively.

#### 4.2. The Magnetic Field on an Arcsecond Scale in W3 IRS 5

Troland et al. (1989), RCTG, and Greaves et al. (1994) found a gradient of the magnetic field along the line of sight and proposed “hourglass” models for the W3 IRS 5 magnetic field on a large scale ( $1'$ ). In these models, an inclination angle of the hourglass major axis  $\theta \simeq 2^\circ$  was adopted with respect to the sky plane on the basis of the angular distribution of the magnetic field strength along the line of sight, which was obtained by RCTG. A position angle of the major axis, P.A.  $\sim 50^\circ$ , and a FWHM width of the pinch, FWHM =  $10''$ , were adopted on the basis of the spatial distribution of the EVPAs, which was obtained by Greaves et al. (1994) with an angular resolution of  $13''.5$ .

In this paper, we propose an hourglass model of the magnetic field shown in Figure 5. This model is made to explain the magnetic field on the small scale ( $<10''$ ) and is consistent

with the large-scale magnetic field ( $\sim 1'$ ) observed by RCTG and Greaves et al. (1994). The modeled field is pinched in at the peak of the  $800 \mu\text{m}$  continuum emission. Ladd et al. (1993) observed the  $450 \mu\text{m}/800 \mu\text{m}$  continuum emission with a  $7''$  beam (a pointing accuracy of  $2''$ ) and found that the peak of the emission has a position offset of about  $-2''.5$  in R.A. and about  $+0''.5$  in decl. with respect to the center of the maser cluster. Although the continuum emission peak should coincide with the  $^{13}\text{CO}$  and  $\text{C}^{18}\text{O}$  emission peaks (Oldham et al. 1994; Tieftrunk et al. 1995; Roberts et al. 1997), the observed position is somewhat uncertain because of the large beams. It is possible that the  $\text{C}^{13}\text{O}$  emission peak observed by Roberts et al. (1997) traces a segment of the outflow while the continuum emission peak traces the densest part of the parent molecular cloud. Tieftrunk et al. (1995) found four gas clumps traced by  $\text{C}^{34}\text{S } J = 3-2$  and  $J = 5-4$  emission, but none of the emission peaks coincides with the pinch center.

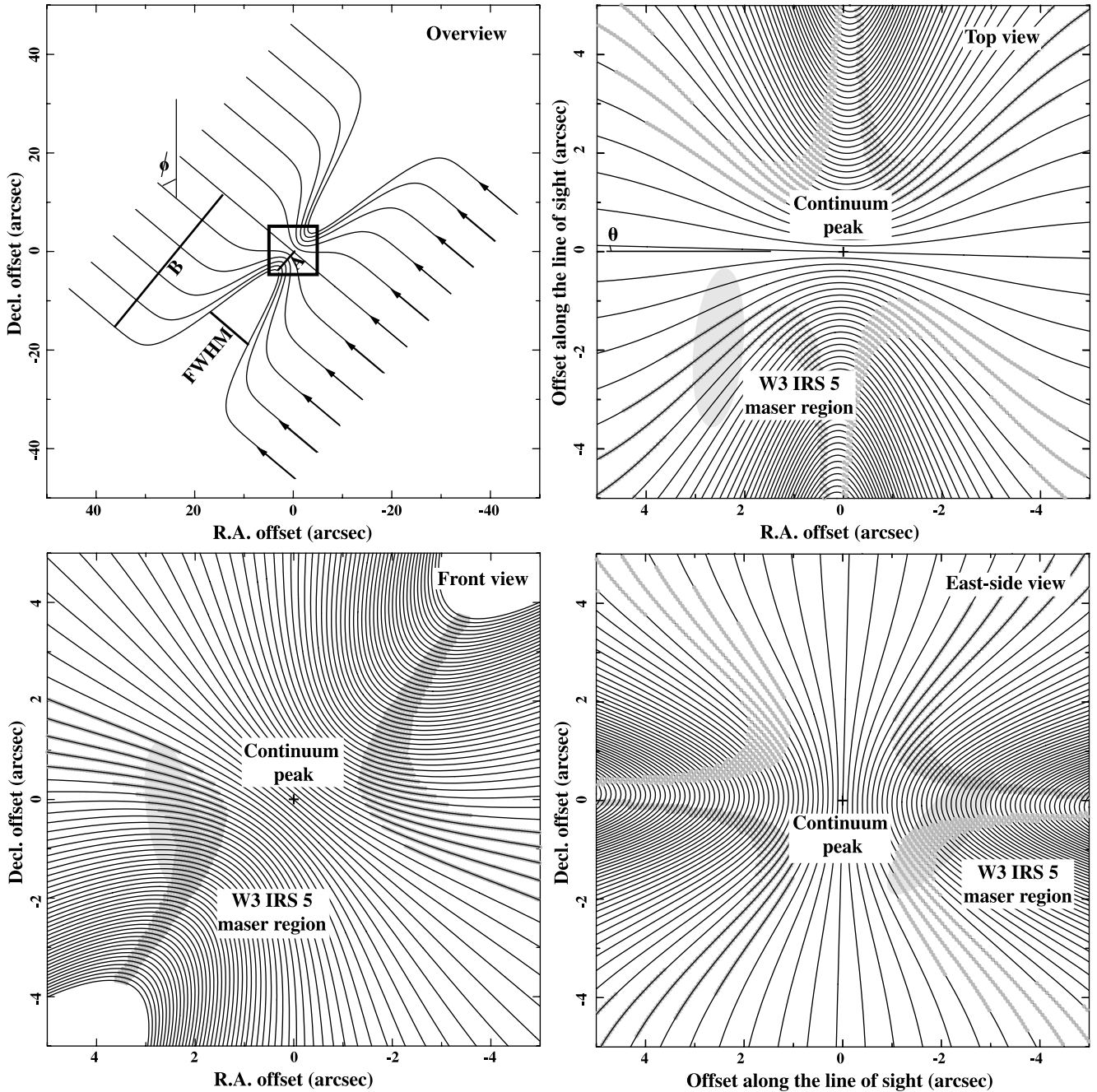


FIG. 5.—Hourglass model of the magnetic field in the W3 IRS 5 region. The angle  $\theta \sim 2^\circ$  is the angle of inclination with respect to the sky plane,  $\phi \sim 50^\circ$  is the position angle,  $A/B$  is the pinch ratio ( $A = 5''$ ,  $B = 35''$ ) and  $\text{FWHM} = 10''$  is the FWHM width of the the pinch at the location of the water masers. All of the definitions are the same as those described in Fig. 7 of Roberts et al. (1993). A square ( $10'' \times 10''$ ) in the overview panel indicates the area zoomed-in and described in the other three subpanels. Thick parts of the magnetic field lines in the zoomed-in front view subpanel indicate the locations where the field line have position angles  $65^\circ \leq \text{P.A.}_M \leq 85^\circ$ . The location and the area of the W3 IRS 5 water maser region are indicated by a filled gray ellipse. The area center is located at  $2''.5$ ,  $-0''.5$ , and  $-2''.0$  in R.A., decl., and line-of-sight offsets, respectively. The orientation of the ellipse major axis indicates the direction of the outflow found in the maser region (see Figs. 6 and 7 of Paper I). Thick parts of the magnetic field lines in the zoomed-in top and east side views indicate the locations where the field lines have inclinations  $45^\circ \leq |\theta_M| \leq 60^\circ$ .

The magnetic field projection on the sky (P.A.  $\sim 76^\circ$ ) mentioned in § 4.1 is well consistent with that in the proposed magnetic field model (see Fig. 5b). Taking into account that the magnetic field vector is oriented toward the observer (a negative value of the measured Zeeman effect: STR; STCR), the maser region is likely located in front of the major axis of the hourglass (see Figs. 5c and 5d). The inclination of the magnetic field to the line of sight, however, cannot be completely consistent with the model, in which

the inclination significantly varies from one point to another in the whole maser region.

The alignment of the magnetic field in the coverage of about  $1'' \times 4''$  in the water maser region provides a constraint on the pinch ratio of the hourglass model around  $A/B \sim 0.14$ , as well as on the pinch width around  $\text{FWHM} \sim 10''$  (definitions of  $A$  and  $B$  are given in the legend of Fig. 5). As discussed by RCTG, one obtains a magnetic field strength of  $\sim 1.3$  mG at the pinch center when

assuming a strength of the total undisturbed magnetic field of  $25 \mu\text{G}$  and considering the  $r^{-2}$  dependence of the magnetic field. This value is 1 order of magnitude smaller than that obtained by STR and STCR ( $\sim 30 \text{ mG}$ ) but 1 order of magnitude larger than that estimated by RCTG. Crutcher (1999) found an empirical relation of magnetic field strength,  $B \propto n^{0.47}$ , over a large range of gas densities  $n$  up to  $10^7 \text{ cm}^{-3}$ . Therefore, it is expected that the field strength found in the water maser cloud ( $n \gtrsim 10^8\text{--}10^9 \text{ cm}^{-3}$ ) is consistent with the  $B$ - $n$  law (cf. STR). STCR also pointed out that the magnetic field in the interstellar space (preshock region) should be enhanced in the maser region (postshock region) by a factor of  $\sim 20$ .

#### 4.3. The Magnetodynamically Supercritical Collapse of the Parent Molecular Cloud of W3 IRS 5

The origin of the magnetic field pinch is still obscured. The direction of the whole magnetic field is almost parallel to a molecular outflow found in W3 A (Mitchell et al. 1991; Hasegawa et al. 1994). Momose et al. (2001) pointed out that a magnetic field would control the direction of a molecular outflow rather than that the magnetic field is influenced by the outflow. In W3 IRS 5, however, although the magnetic field seems to along the molecular outflow on a larger scale ( $\sim 1'$ ), it may not necessarily be parallel to the outflows on a smaller scale ( $\sim 5''$ ) as seen in the water masers. We evaluated the energy densities of the magnetic field and of the outflow of W3 IRS 5 using the same equations described in Momose et al. (2001). The critical magnetic field strength,  $B_{\text{critical}}$ , at which the field has the same energy density as that of the cylindrical outflow, is expressed by

$$B_{\text{critical}} = \left( \frac{8E_{\text{flow}}}{r^2 l} \right)^{1/2}, \quad (2)$$

where  $E_{\text{flow}}$ ,  $r$ , and  $l$  are the kinetic energy, the radius, and the total length of the cylindrical outflow, respectively. Adopting the total outflow energy estimated by Hasegawa et al. (1994),  $E_{\text{flow}} \simeq 1.2 \times 10^{46}$  ergs, and the radius and the length of the outflow estimated by Mitchell et al. (1991),  $r \simeq 4.1 \times 10^{17}$  cm and  $l \simeq 2.5 \times 10^{18}$  cm, respectively (assuming the distance to W3 IRS 5 of 1.8 kpc here), we obtained  $B_{\text{critical}} \simeq 0.48 \text{ mG}$ , which is larger than the maximum strength observed in the H I Zeeman effect by RCTG ( $\lesssim 0.22 \text{ mG}$ ). To obtain  $B_{\text{critical}}$  for the water maser cloud, we converted equation (2) to

$$B_{\text{critical}} = (8\pi\rho_{\text{maser}}v_{\text{maser}}^2)^{1/2}, \quad (3)$$

where  $\rho_{\text{maser}} \gtrsim 3.3 \times 10^{-14} \text{ g cm}^{-3}$  (corresponding to  $n_{\text{H}_2} = 10^8 \text{ cm}^{-3}$ ) is the gas density of the maser region necessary for maser excitation and  $v_{\text{maser}}$  is the outflow velocity. Adopting the outflow velocity  $v_{\text{maser}} \sim 15 \text{ km s}^{-1}$ , we obtained  $B_{\text{critical}} \simeq 250 \text{ mG}$ . Thus, the magnetic field strength estimated on the basis of the Zeeman splitting ( $\simeq 30 \text{ mG}$ ; STR) is 1 order of magnitude lower than the critical strength. This suggests that the magnetic field cannot control the outflow dynamics.

This evaluation is consistent with that made for the W51 M region by LLD. On the other hand, there is no observational evidence that the outflow controls the magnetic field structure. Momose et al. (2001) suggested that the magnetic field is aligned more in the younger phase of star formation than in the more evolved one, so the disturbance of the

former magnetic field due to the small-scale turbulence is not significant yet. This suggestion supports the idea that W3 IRS 5 should be at the very early stage of star formation. Oldham et al. (1994) and Tieftrunk et al. (1995) estimated the mass of the molecular cloud associated with W3 IRS 5 to be  $800\text{--}900 M_{\odot}$ . This value is still larger than the magnetodynamically critical mass of  $510 M_{\odot}$  for a cloud with a radius of 9000 AU (corresponding to  $5''$  at 1.8 kpc) and a magnetic field strength of  $30 \text{ mG}$ . This indicates that the magnetic field of the W3 IRS 5 cannot support the gravity of the molecular cloud, in other words, that a part of the W3 IRS 5 cloud is collapsing under the magnetodynamically supercritical condition (Shu et al. 1987).

Note that the above evaluation is still consistent with the suggestion that the magnetic field should control the water maser excitation (Elitzur et al. 1989, 1992; STCR). To consider the maser excitation, the velocity dispersion of the postshock region where the masers are excited,  $\sigma_v \lesssim 0.6 \text{ km s}^{-1}$ , is inserted instead of  $v_{\text{maser}}$  in equation (3) (Papers I and II; STCR). Then one can estimate  $B_{\text{maser}} \simeq 10 \text{ mG}$ , which is smaller than or equal to the observed magnetic field strength.

It is still unclear what kind of object exists in the pinch center of the magnetic field. Tieftrunk et al. (1995) found four molecular gas clumps in W3 IRS 5, but none of the clumps is located at the pinch center. It is likely that these clumps were formed in the common parent molecular cloud and are responsible for the observed magnetic field. The magnetic field that controlled the multiple clumps supports the mild pinch ratio  $A/B \simeq 0.14$  rather than the extremely small ratio  $A/B \simeq 0.04$  speculated on by RCTG.

## 5. SUMMARY

Polarimetric VLBI observations of water masers in W3 IRS 5 have revealed that observed EVPAs of water masers features are well aligned in the whole maser region except for a small number of maser features. The directions of the magnetic field projected on the sky in the maser region are estimated to be perpendicular to the directions of the linear polarization of the masers (P.A.  $\sim 76^\circ$ ). The magnetic field estimated supports the hourglass magnetic field model proposed previously. Thus, water maser linear polarization may reveal in detail the magnetic fields of the interstellar medium in star-forming regions. The W3 IRS 5 water maser region has a position offset from the pinch center of the hourglass, and its magnetic field is unlikely to control the outflow dynamics. All of these observational facts suggest that the W3 IRS 5 cloud is collapsing under the magnetically supercritical condition and that the outflows are not yet developed enough to completely disturb the magnetic field in this cloud. The hourglass structure of the magnetic field is suggested to be formed as a result of the collapse of the parent molecular cloud that is magnetically supercritical.

The authors acknowledge Dr. Chris Carilli for helping our VLBA and VLA observations as a technical contact person. The authors also thank Drs. Tetsuo Sasao, Makoto Miyoshi, and Yoshiharu Asaki for helping with the VLBA observation and Motohide Tamura for providing fruitful information on interstellar polarimetric data. H. I. was financially supported by the Research Fellowship of the Japan Society for the Promotion of Science for Young Scientists.

## REFERENCES

- Abraham, Z., & Vilas Boas, J. W. S. 1994, *A&A*, 290, 956
- Akujor, C. E., Spencer, R. E., Zhang, F. J., Fanti, C., Ludke, E., & Garrington, S. T. 1993, *A&A*, 274, 752
- Barvainis, R., & Deguchi, S. 1989, *AJ*, 97, 1089
- Claussen, M. J., Gaume, R. A., Johnston, K. J., & Wilson, T. L. 1994, *ApJ*, 424, L41
- Crutcher, R. M. 1999, *ApJ*, 520, 706
- Deguchi, S., & Watson, W. D. 1986a, *ApJ*, 302, 750
- . 1986b, *ApJ*, 302, 108
- . 1990, *ApJ*, 354, 649
- Diamond, P. J. 1995, in *ASP Conf. Ser. 82, Very Long Baseline Interferometry and the VLBA*, ed. J. A. Zensus, P. J. Diamond, & P. J. Napier (San Francisco: ASP), 227
- Elitzur, M. 1992a, *Astronomical Masers* (Dordrecht: Kluwer)
- . 1992b, *ARA&A*, 30, 75
- Elitzur, M., Hollenbach, D. J., & McKee, C. F. 1989, *ApJ*, 346, 983
- . 1992, *ApJ*, 394, 221
- Evans, N. J., II. 1999, *ARA&A*, 37, 311
- Feigelson, E. D., & Montmerle, T. 1999, *ARA&A*, 37, 363
- Genzel, R., & Downes, D. 1977, *A&AS*, 30, 145
- Goldreich, P., Keeley, D. A., & Kwan, J. Y. 1973, *ApJ*, 179, 111
- Greaves, J. S., Murray, A. G., & Holland, W. S. 1994, *A&A*, 284, L19
- Gwinn, C. R. 1994a, *ApJ*, 429, 241
- . 1994b, *ApJ*, 429, 253
- Gwinn, C. R., Moran, J. M., & Reid, M. J. 1992, *ApJ*, 393, 149
- Hasegawa, T. I., Mitchell, G. F., Matthews, H. E., & Tacconi, L. 1994, *ApJ*, 426, 215
- Hayashi, M., Kobayashi, H., & Hasegawa, T. 1989, *ApJ*, 340, 298
- Heiles, C., Goodman, A. A., McKee, C. F., & Zweibel, E. G. 1993, in *Protostar and Planets III*, ed. E. H. Levy & J. I. Lunine (Tucson: Univ. Arizona Press), 279
- Hollenbach, D. J., Elitzur, M., & McKee, C. F. 1993, in *Astrophysical Masers*, ed. A. W. Clegg & G. E. Nedoluha (Heidelberg: Springer), 159
- Hollenbach, D., & McKee, C. F. 1989, *ApJ*, 342, 306
- Horiuchi, S., & Kameya, O. 2000, *PASJ*, 52, 545
- . 2003, in *IAU Symp. 206, Cosmic Masers: From Protostars to Black Holes*, ed. V. Migenes & M. J. Reid (San Francisco: ASP), 92
- Horiuchi, S., Migenes, V., & Deguchi, S. 2000, in *Astrophysical Phenomena Revealed by Space VLBI*, Proceedings of the VSOP Symposium, ed. H. Hirabayashi, P. G. Edwards, & D. W. Murphy (Sagamihara: ISAS), 105
- Imai, H., Deguchi, S., & Sasao, T. 2002, *ApJ*, 567, 971 (Paper II)
- Imai, H., Kameya, O., Sasao, T., Miyoshi, M., Deguchi, S., Horiuchi, S., & Asaki, Y. 2000, *ApJ*, 538, 751 (Paper I)
- Ladd, E. F., Deane, J. R., Sanders, D. B., & Wynn-Williams, C. G. 1993, *ApJ*, 419, 186
- Leppänen, K., Liljeström, T., & Diamond, P. J. 1998, *ApJ*, 507, 909 (LLD)
- Marscher, A. P., Jorstad, S. G., Mattox, J. R., & Wehrle, A. 2002, *ApJ*, 577, 85
- Matveyenko, L. I., Diamond, P. J., & Graham, D. A. 2003, in *IAU Symp. 206, Cosmic Masers: From Protostars to Black Holes*, ed. V. Migenes & M. J. Reid (San Francisco: ASP), 96
- McKee, C. F., Zweobe, E. G., Godman, A. A., & Heiles, C. 1993, in *Protostar and Planets III*, ed. E. H. Levy & J. I. Lunine (Tucson: Univ. Arizona Press), 327
- Mitchell, G. F., Maillard, J.-P., & Hasegawa, T. I. 1991, *ApJ*, 371, 342
- Momose, M., Tamura, M., Kameya, O., Greaves, J. S., Chrysotomou, A., Hough, J. H., & Morino, J.-I. 2001, *ApJ*, 555, 855
- Oldham, P. G., Griffin, M. J., Richardson, K. J., & Sandell, G. 1994, *A&A*, 284, 559
- Reid, M. J. 1995, in *ASP Conf. Ser. 82, Very Long Baseline Interferometry and the VLBA*, ed. J. A. Zensus, P. J. Diamond, & P. J. Napier (San Francisco: ASP), 209
- Reid, M. J., & Moran, J. M. 1981, *ARA&A*, 19, 231
- Roberts, D. A., Crutcher, R. M., & Troland, T. H. 1997, *ApJ*, 479, 318
- Roberts, D. A., Crutcher, R. M., Troland, T. H., & Goss, W. M. 1993, *ApJ*, 412, 675 (RCTG)
- Sarma, A. P., Troland, T. H., Crutcher, R. M., & Roberts, D. A. 2002, *ApJ*, 580, 928 (STCR)
- Sarma, A. P., Troland, T. H., & Romney, J. D. 2001, *ApJ*, 554, L217 (STR)
- Shu, F. H., Adams, F. C., & Lizano, S. 1987, *ARA&A*, 25, 23
- Tieftrunk, A. R., Gaume, R. A., Claussen, M. J., Wilson, T. L., & Johnston, K. J. 1997, *A&A*, 318, 931
- Tieftrunk, A. R., Wilson, T. L., Steppe, H., Gaume, R. A., Johnston, K. J., & Claussen, M. J. 1995, *A&A*, 303, 901
- Torrelles, J. M., et al. 2001a, *Nature*, 411, 277
- . 2001b, *ApJ*, 560, 853
- Troland, T. H., Crutcher, R. M., Goss, W. M., & Heiles, C. 1989, *ApJ*, 347, L89